A study of the 15-μm quasars in the ELAIS N1 and N2 fields

Article (Published Version)

Mon. Not. R. Astron. Soc. **354,** 961–970 (2004) doi:10.1111/j.1365-2966.2004.08264.x

A study of the 15-μm quasars in the ELAIS N1 and N2 fields

A. Afonso-Luis,[1⋆] E. Hatziminaoglou,[1] I. Pérez-Fournon,[1] E. A. González-Solares,[2] M. Rowan-Robinson,[3] M. Vaccari,[3] C. Lari,[4] S. Serjeant,[5] S. Oliver,[6] A. Hernán-Caballero[1] and F. M. Montenegro-Montes[1]

[1]*Instituto de Astrofisica de Canarias, C/Via Lactea s/n, E-38200 La Laguna, Spain*
[2]*Institute of Astronomy, University of Cambridge, Madingley Road, Cambridge CB3 0HA*
[3]*Imperial College of Science, Technology and Medicine, Prince Consort Road, London SW7 2BZ*
[4]*Instituto de Radioastronomia, Via P. Gobetti 101, Bologna 40129, Italy*
[5]*Centre for Astrophysics and Planetary Science, School of Physical Sciences, University of Kent, Canterbury CT2 7NR*
[6]*Astronomy Centre, Department of Physics and Astronomy, University of Sussex, Falmer, Brighton BN1 9QJ*

Accepted 2004 July 27. Received 2004 July 27; in original form 2004 May 21

ABSTRACT

This paper discusses the properties of the European Large Area *ISO* Survey (ELAIS) 15-μm quasars and tries to establish a robust method of quasar selection for future use within the *Spitzer* Wide-Area Infrared Extragalactic Survey (SWIRE) framework. The importance of good-quality ground-based optical data is stressed, both for the selection of candidates and for the estimation of photometric redshifts. Colour–colour plots and template fitting are used for these purposes. The properties of the 15-μm quasar sample, including variability and black hole masses, are studied and compared to the properties of other quasars that lie within the same fields but have no mid-infrared counterparts. The two subsamples do not present substantial differences and are believed to come from the same parent population.

Key words: techniques: photometric – quasars: emission lines – quasars: general – infrared: general.

1 INTRODUCTION

The European Large Area *ISO* Survey (ELAIS, Oliver et al. 2000) is the largest survey performed with the *Infrared Space Observatory* (*ISO*, Kessler et al. 1996) at 6.7, 15, 90 and 175 μm, and has resulted in the delivery of the largest catalogue of any *ISO* survey (Rowan-Robinson et al. 2004) from both the ISOCAM (Cesarsky et al. 1996) and ISOPHOT (Lemke et al. 1996) instruments. In particular, the 15-μm survey (performed with the ISOCAM instrument) covers an area of $\sim$12 deg^2, divided into four main fields (N1, N2, N3 and S1) and several smaller areas. The 15-μm observations in the four main fields were analysed by Vaccari et al. (2004), providing a catalogue of 1923 sources detected with signal-to-noise ratio S/N $>$ 5 over 10.85 deg^2. The Final Band-Merged Catalogue (Rowan-Robinson et al. 2004) combines all source lists at different wavelengths and redshifts obtained to date in ELAIS fields. This catalogue comprises a total of 3523 entries, with about one-third having spectroscopic identifications.

Owing to the fact that complete spectroscopic follow-up is usually not feasible over large and deep fields, one needs to use tools for detecting quasar candidates using photometric data only. As part of our study of mid-infrared (IR) quasars, we present the results of two independent quasar candidate selection techniques, one based on colour–colour diagrams and the other one on template fitting, and try to improve the selection including IR constraints. In recent years, with the available multicolour surveys, quasar photometric redshift methods have been developed, but they yield somewhat less reliable results than those for galaxies (e.g. Hatziminaoglou, Mathez & Pelló 2000; Richards et al. 2001). For the purposes of this work, the template fitting technique (Hatziminaoglou et al. 2000) is applied on the two different data sets available for the studied fields (SDSS and WFS). All methods and results described in this paper can be directly applied to the *Spitzer* Wide-Area Infrared Extragalactic Survey (SWIRE, Lonsdale et al. 2003).

The layout of this paper is as follows. In Section 2 a brief description of the optical data available for this work is given. Section 3 deals with variability issues. In Section 4 a description of the selection of quasar candidates using optical and IR properties is given, based on two different methods. Photometric redshifts for the spectroscopically confirmed quasars in the two data sets (SDSS and WFS) are estimated and the results obtained for the two photometric systems are discussed. Section 5 compares the results for the sources with and without IR counterparts, in terms of their statistical properties and black hole (BH) masses. Our conclusions are presented in Section 6.

2 THE 15-μm QUASAR SAMPLE AND RELATED OPTICAL DATA

In the present work we study the Type I quasars detected by *ISO* at 15 μm in two of the ELAIS fields, N1 and N2. Throughout this

⋆E-mail: aal@iac.es

work, the traditional (but conservative) requirement of a quasar to be point-like has been set, and sources classified as extended based on their *r*-band morphology are not taken into account. The morphological selection is made in order to avoid contamination by galaxies of the quasar candidate samples discussed in Section 4 and has no impact on the validity of the results presented here. Out of the 1056 sources in N1 and N2 contained in the ELAIS 15-μm Final Analysis Catalogue Version 1.0 (Vaccari et al. 2004), 849 sources were identified in Isaac Newton Telescope (INT) WFS images by González-Solares et al. (2004), the non-identification being due to either incomplete optical coverage of the 15-μm fields or optical limiting magnitude.

The ELAIS N1 and N2 fields have been fully covered by the Wide Field Survey (WFS, McMahon et al. 2001), carried out with the prime focus Wide Field Camera (WFC) at the 2.5-m Isaac Newton Telescope (INT) at La Palma. The survey consists of single 600-s exposures in five bands, *U*, *g*, *r*, *i* and *z*, down to AB magnitude limits (5σ limits for a point source) of 24.1, 24.8, 24.1, 23.6 and 22.4, respectively. The AB corrections for the conversion from the (original) Vega magnitudes to AB magnitudes have been computed using HyperZ (Bolzonella, Miralles & Pelló 2000) and are 0.751, −0.063, 0.165, 0.407 and 0.534 for *U*, *g*, *r*, *i* and *z*, respectively. Out of the 849 sources detected in 15 μm in N1 and N2, there are 110 point sources (SExtractor CLASS_STAR $\geqslant 0.9$), excluding saturated stars, with emission at 15 μm (González-Solares et al. 2004).

In addition to WFS, the Sloan Digital Sky Survey (SDSS) has validated and made publicly available its Data Release 1 (DR1, Abazajian et al. 2003), partially covering our fields. SDSS consists of five-band (*u*, *g*, *r*, *i*, *z*) imaging data covering 2099 deg^2, 186 240 spectra of galaxies, quasars, stars and calibrating blank sky patches selected over 1360 deg^2 of this area, and catalogues of measured parameters from these data. The imaging data reach a limiting AB magnitude (Vanden Berk et al. 2004) of $r \sim 22.6$ (95 per cent completeness limit for stars). Among the 15-μm sources in the areas covered by the SDSS DR1 photometry, 82 have been morphologically classified as point sources (SDSS OBJC_TYPE = 6). In fact, the partial coverage of N1 and N2 provides photometry and spectra for a variety of sources. More particularly, among the 36 SDSS spectroscopically confirmed quasars lying in the N1 and N2 fields, 16 have been detected at 15 μm. Note, however, that the areas covered by spectroscopy do not exactly coincide with those covered by photometry and are, in fact, smaller. Two morphologically extended low-redshift quasars (0.214 and 0.245) with *r*-band magnitudes of 18.25 and 18.58 have been excluded from the spectroscopically confirmed quasar sample, for the reasons mentioned at the beginning of this section. Throughout this work and unless otherwise stated, all magnitudes will refer to the AB system.

Fig. 1 shows the coverage of the ELAIS N1 and N2 fields by the WFS and the SDSS DR1 photometric and spectroscopic data.

Finally, as a part of the extensive programme of ground-based spectroscopy associated with the ELAIS survey, there have been follow-up observations of ELAIS 15-μm sources in the N1 and N2 fields (Pérez-Fournon et al., in preparation) using the WYFFOS multifibre spectrograph, on the William Herschel Telescope (WHT) at La Palma. This observing run added nine previously unknown quasars to the spectroscopic sample in the regions of N1 and N2 not covered by the spectroscopic DR1.

Therefore, a total of 25 spectroscopically confirmed quasars have been identified among the final ELAIS 15-μm catalogue and their properties are described in Table 1. Fig. 2 shows the 15-μm flux versus *r*-band flux for the quasar sample.

3 VARIABILITY

Variations in the luminosity of quasars have been observed from X-ray to radio wavelengths, with time-scales of minutes to years. The majority of quasars have continuum variability of the order of 10 per cent on time-scales of months to years (Vanden Berk et al. 2004). Furthermore, recent observations of radio-quiet quasars indicate that more than 80 per cent show long-term (monthly to yearly) variability, with amplitudes up to half a magnitude (Huber et al. 2002). Variability is wavelength-dependent. The continuum ($F_\nu \propto \nu^{-\alpha}$) tends to get harder (the spectral index, α, decreases) as the quasar gets brighter, which means that the variations are larger at shorter wavelengths.

The SDSS imaging strategy consists in observing in almost simultaneous mode the same field in the five different bands. The imaging strategy of the WFS was, however, different, and the same fields were observed in the different filters on time-scales ranging from a few months to more than a year. Fig. 3 shows the differences of the magnitudes for the point sources lying in the common area in the two photometric systems. The magnitude differences show very small dispersions down to a certain magnitude for almost all point sources that are identified as stars, but large variations appear in the case of many of the confirmed quasars (red crosses) in all filters but especially in the *U* and *g* bands, indicating variability-related issues.

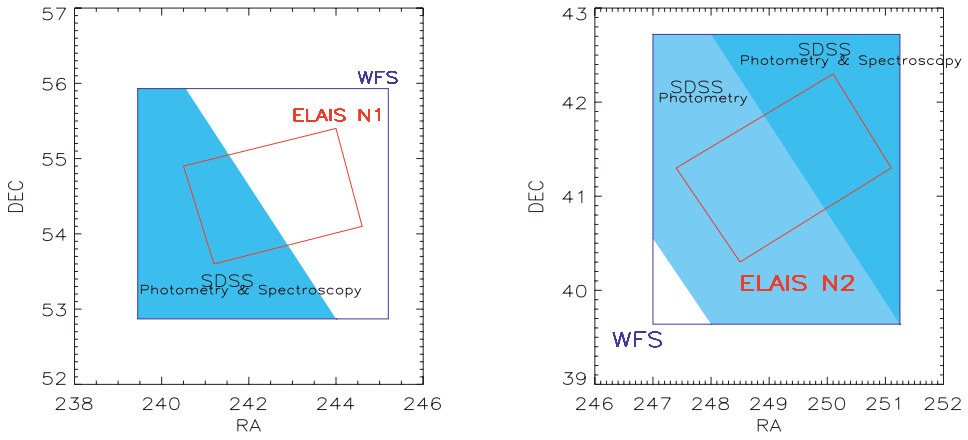

Figure 1. Coverage of the ELAIS N1 and N2 fields (small inner red rectangles) by the WFS and the SDSS DR1 photometric and spectroscopic data.

Table 1. ELAIS 15-μm spectroscopically confirmed quasars. The *r*-band magnitude in column 5 is the SDSS *r*-band magnitude, apart from the objects marked with an asterisk. These objects are outside the spectroscopic coverage of DR1 and the magnitude shown is the WFS *r* magnitude. The last column refers to the origin of the spectra: SDSS from Abazajian et al. (2003); WYFFOS from Pérez-Fournon et al. (in preparation).

ELAIS ID	RA (optical)	Dec. (optical)	*z*	*r* mag.	15-μm flux (mJy)	*z* reference
ELAISC15_J160250.9+545057	240.712 341 31	54.849 472 05	1.1971	19.22	2.1820	SDSS
ELAISC15_J160522.9+545613	241.346 405 03	54.937 084 20	0.5722	18.94	2.2160	SDSS
ELAISC15_J160623.5+540556	241.598 220 83	54.098 888 40	0.8766	17.62	4.2930	SDSS
ELAISC15_J160630.5+542007	241.627 548 22	54.335 441 59	0.8205	18.73	3.4460	SDSS
ELAISC15_J160638.0+535009	241.657 791 14	53.835 720 06	2.9426	19.77	1.6010	SDSS
ELAISC15_J161007.2+535814	242.529 602 05	53.970 554 35	2.0317	18.86	1.7400	SDSS
ELAISC15_J163702.2+413022	249.259 307 86	41.506 168 37	1.1783	19.11	2.0920	SDSS
ELAISC15_J163709.2+414031	249.288 909 91	41.675 197 60	0.7602	17.20	8.4090	SDSS
ELAISC15_J163739.3+414348	249.414 367 68	41.729 999 54	1.4136	18.94	1.0610	SDSS
ELAISC15_J163847.5+421141	249.697 601 32	42.194 946 29	1.7786	18.93	1.7420	SDSS
ELAISC15_J163915.9+412834	249.815 917 97	41.476 028 44	0.6919	19.05	3.3730	SDSS
ELAISC15_J163930.8+410013	249.878 448 49	41.003 807 07	1.0515	18.23	1.2580	SDSS
ELAISC15_J163952.9+410346	249.970 230 10	41.062 442 78	1.6050	18.58	2.0940	SDSS
ELAISC15_J164010.1+410521	250.042 251 59	41.089 553 83	1.0990	17.01	9.5570	SDSS
ELAISC15_J164016.0+412102	250.067 016 60	41.350 387 57	1.7570	18.44	2.0900	SDSS
ELAISC15_J164018.4+405812	250.076 416 02	40.970 306 40	1.3175	18.13	3.7700	SDSS
ELAISC15_J161521.8+543148	243.840 774 54	54.530 166 63	0.4737	18.24*	3.492	WYFFOS
ELAISC15_J161526.7+543004	243.860 946 66	54.501 750 95	1.3670	19.35*	1.457	WYFFOS
ELAISC15_J161543.5+544828	243.931 335 45	54.807 998 66	1.6920	18.22*	2.107	WYFFOS
ELAISC15_J163425.2+404152	248.604 721 07	40.697 944 64	1.6840	18.37	3.1690	WYFFOS
ELAISC15_J163502.7+412953	248.761 764 53	41.498 085 02	0.4727	18.08	2.1730	WYFFOS
ELAISC15_J163531.1+410025	248.879 562 38	41.007 610 32	1.1500	18.81	1.3990	WYFFOS
ELAISC15_J163533.9+404025	248.891 769 41	40.673 805 24	0.5340	19.72	2.7300	WYFFOS
ELAISC15_J163553.5+412054	248.973 541 26	41.348 831 18	1.1950	19.39	2.7260	WYFFOS
ELAISC15_J163634.4+412742	249.143 432 62	41.462 001 80	0.1711	18.50	4.1540	WYFFOS

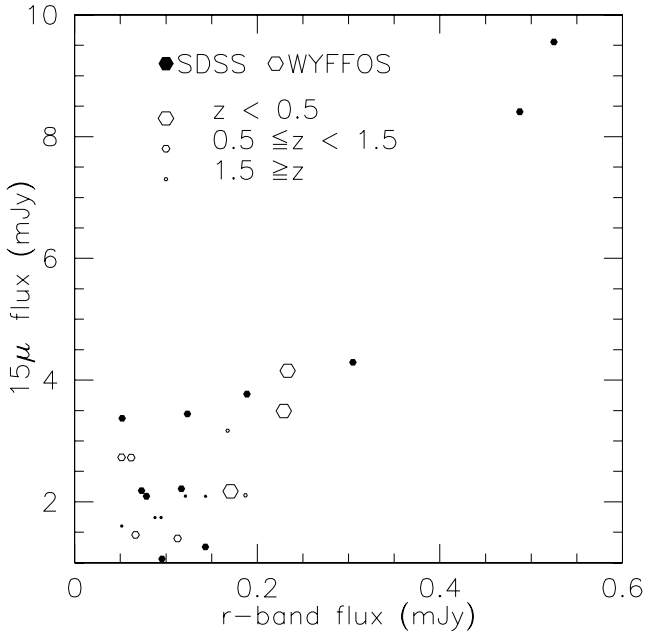

Figure 2. Plot of *r*-band versus 15-μm flux for the quasar sample. Filled (open) circles represent objects with SDSS (WYFFOS) spectra. Symbol size decreases with increasing redshift.

It might be argued that the variations are due to the different photometric systems, however close they may be. For this purpose, a simulated quasar catalogue was created, based on the colours of the SDSS composite quasar spectrum (Vanden Berk et al. 2001), including all 10 filters and for redshifts spanning from 0 to 6, and the magnitudes were compared. Fig. 4 illustrates the expected magnitude differences as a function of magnitude for redshifts in the interval [0, 4], where all our spectroscopically confirmed quasars lie, and for the filters *U*, *g* and *z*. Filters *r* and *i* were omitted for clarity as the points largely overlap with the rest of the points. Even though magnitude variations are predicted, their amplitude is significantly smaller than the ones observed. We therefore conclude that not all observed variations between the SDSS and WFS photometry can be explained by the differences of the photometric systems and that some must be a result of quasar variability.

This strongly suggests that quasar candidate selection and photometric redshift estimates are likely not to be accurate for all objects when WFS or other similar data are used and additional methods have to be looked for.

4 QUASAR CANDIDATE SELECTION

For the purpose of identifying high-probability quasar candidates from the available data sets, we used two techniques: a combination of colour–colour diagrams (hereafter method 1, M1) and the template fitting method (method 2, M2). M1, based on Richards et al. (2002), consists of a colour–colour selection algorithm trained using the SDSS Early Data Release (Stoughton et al. 2002), for low- to intermediate-redshift (∼2.5) objects. M2 is the standard template fitting that simultaneously provides a photometric redshift estimate for the quasar candidates. The point-source template library comprises quasar and stellar templates, and the observed spectral energy distribution (SED) of each object is compared with the one computed

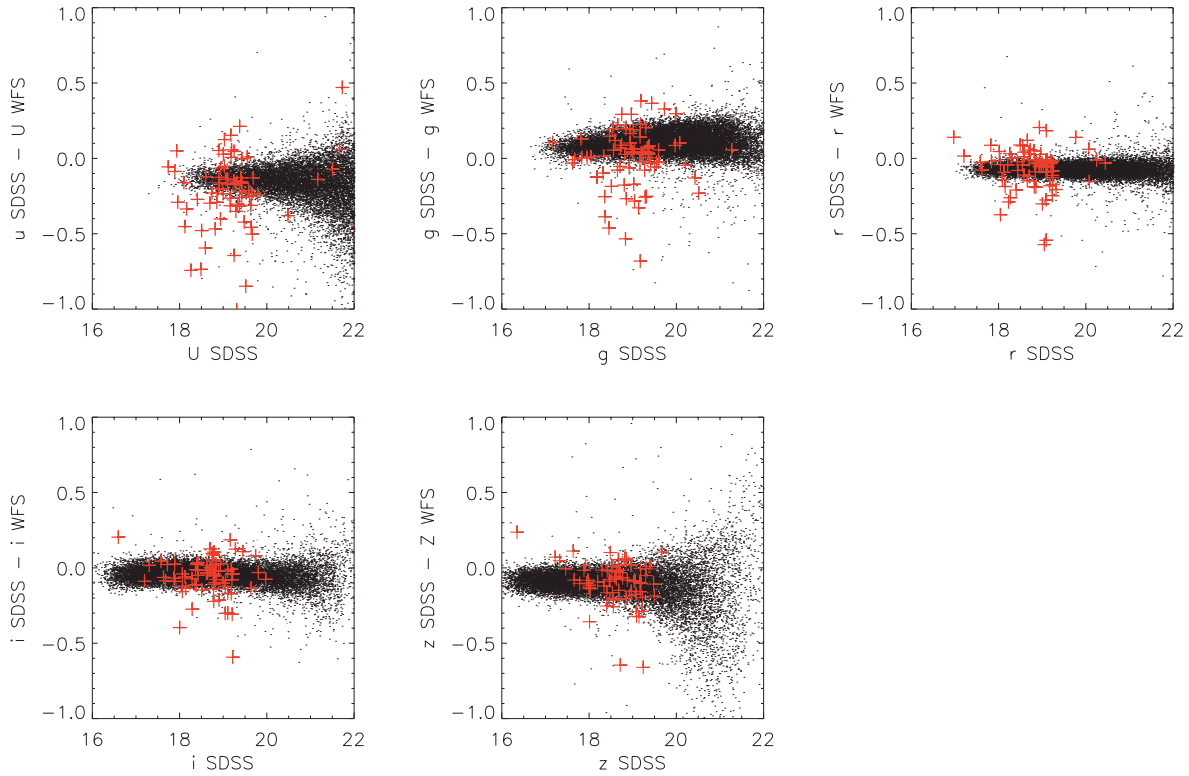

Figure 3. Magnitude differences between SDSS and WFS. The black dots represent the point sources, mostly stars, while the red crosses indicate the 73 confirmed quasars. The photometric errors for the quasars are lower than 0.05 mag in all bands and the dispersion in their magnitudes is evident.

by convolving each template with the transmissions of the filters (for further details see Hatziminaoglou et al. 2000, 2002). M1 is expected to give higher confirmation rates (i.e. number of real quasars over the number of quasar candidates) at low and intermediate redshifts, but its efficiency greatly depends on the photometric system used and cannot be applied as such when other filters are used. M2 is subject to higher contamination from sources other than quasars (e.g. stars) but is expected to have a much better efficiency at high redshift and can be used for any filter combination. In order to improve the results, we also make use of the IR information available for the 15-μm sources keeping in mind that the combination of all these techniques will be applied in the near future in the framework of SWIRE.

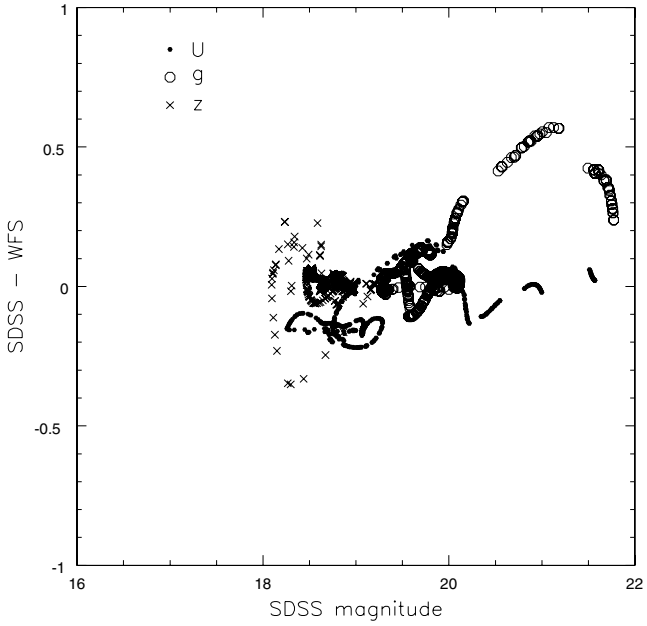

Figure 4. Theoretical magnitude differences for the filters U, g and z of the SDSS and WFS photometric systems, in the redshift interval [0, 4]. Filters r and i have been omitted for clarity.

A first test is made using the more reliable SDSS photometry (Section 4.1), but an attempt to select candidates based on the WFS photometry will also be presented (Section 4.2). Our test sample consists of 21 spectroscopically confirmed quasars with available SDSS photometry and 25 with WFS photometry, which include all 21 from SDSS (see Table 1). Fine-tuning the method for WFS data is very important, as a large part of the SWIRE fields have been observed by the WFS.

4.1 Quasar candidates with SDSS photometry

A sample of 82 ELAIS sources at 15 μm identified as point sources from their optical photometry (SDSS OBJC_TYPE = 6) with r-band magnitudes brighter that 22.6 has been selected from the SDSS photometric catalogue. The optical magnitude cut has been imposed in order to avoid spurious detections and large photometric errors.

The 15-μm information can be used in order to impose IR conditions in the selection of quasar candidates. Stars, galaxies and active galactic nuclei (AGN) all have different optical to mid-IR slopes, with stars typically having larger optical than mid-IR fluxes (González-Solares et al. 2004). Furthermore, according to models of galaxies in the IR (Rowan-Robinson 2001), quasar mid-IR fluxes

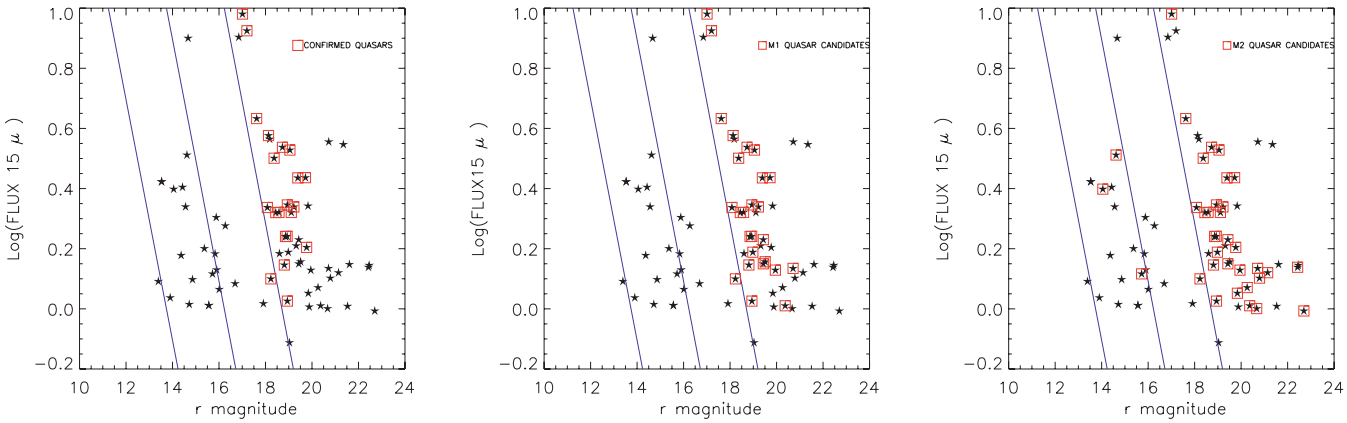

Figure 5. Plots of 15-μm flux (mJy) versus SDSS *r*-band magnitude for the point sources (stars) within the parts of ELAIS N1 and N2 areas covered by SDSS. The red open squares indicate the confirmed quasars (left-hand panel), M1 quasar candidates (central panel) and M2 quasar candidates (right-hand panel). The blue lines represents constant 15-μm to *r*-band flux, with values 0.1, 1.0 and 10.

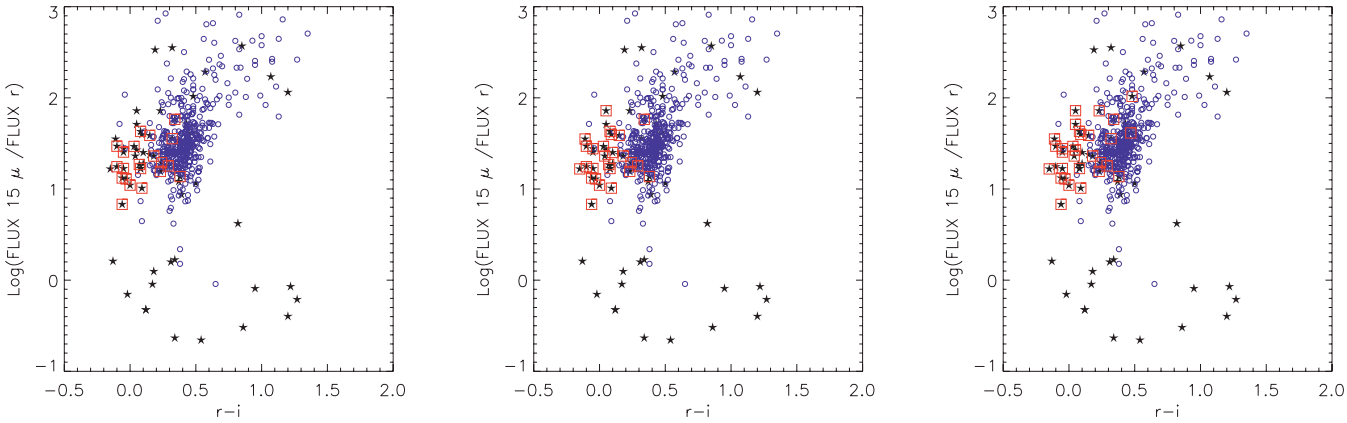

Figure 6. Plots of 15-μm to *r*-band flux versus SDSS $r - i$ for the point sources (stars) and extended sources (open circles). The red open squares indicate spectroscopically confirmed quasars (left-hand panel), M1 quasar candidates (central panel) and M2 quasar candidates (right-hand panel).

are some 10–100 times larger than their optical ones. Taking this into account, one can impose additional constraints on the selection criteria requiring a mid-IR to optical flux ratio of at least 10 for quasar candidates (hereafter condition 1, C1). This condition allows the removal of three quasar candidates selected by M2 that have mid-IR to optical fluxes like those of stars. Fig. 5 illustrates the positions of the different object types and the regions where quasars and quasar candidates selected by the two methods lie.

In order to distinguish between quasars and galaxies, one can make a combined use of optical and optical/IR colours, taking advantage of the fact that quasars up to a redshift of ∼3 are typically bluer than galaxies (González-Solares et al. 2004). Furthermore, 97.55 per cent of all spectroscopically confirmed quasars in the DR1 quasar catalogue (Schneider et al. 2003) have $r - i < 0.52$ (hereafter condition 2, C2). Fig. 6 shows the distribution of stars (lower mid-IR to optical fluxes), galaxies and quasars (bluer than galaxies in general). Marked in red open squares are the spectroscopically confirmed quasars (left-hand panel) and the candidates selected by methods M1 and M2 (middle and right-hand panels, respectively). As can be seen, all the spectroscopically confirmed quasars form a clump bluewards of $r - i \sim 0.52$. In this particular case, C2 does not improve the results of any of the methods but will be used further on.

Table 2. Comparison of the completeness and confirmation rate yielded by M1 and M2 on a sample of 82 SDSS point sources with 15-μm emission. The second column shows the number of quasar candidates (N_c) and the number of spectroscopically confirmed quasars among them (N_f).

Method	N_c (N_f)	Completeness	Conf. rate
M1	26 (19)	90 per cent	73 per cent
M2	33 (19)	90 per cent	58 per cent
M2 + C1	30 (19)	90 per cent	63 per cent

If N_c is the number of quasar candidates stemming from the identification technique, N_f the number of real quasars among the candidates, and N_e the number of expected (based on models) or known (based on complete observations) quasars, then the *completeness* and *confirmation rate* can be defined as N_f/N_e and N_f/N_c, respectively (Hatziminaoglou et al. 2000). Table 2 compares the two quantities yielded by the two methods. Both methods give the same completeness, but the colour–colour selection favours the confirmation rate. Note, however, that the values given here for confirmation rate are *lower limits*. A substantial number of candidates (some 30 per cent) are fainter than the SDSS spectroscopic completeness limit or lie outside the area covered by spectroscopy and

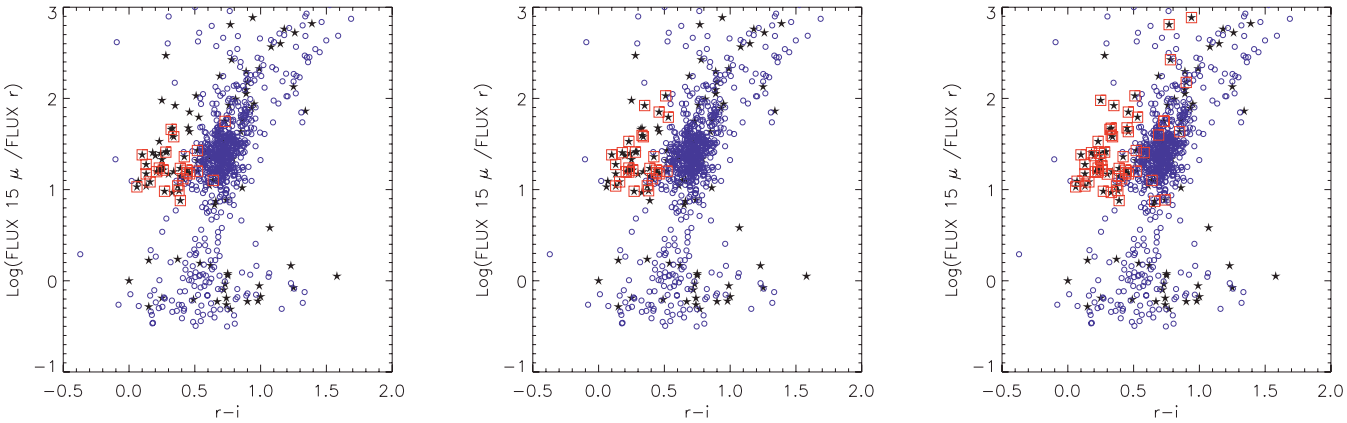

Figure 7. Plots of 15-μm to *r*-band flux versus WFS $r - i$ for the point sources (stars) and extended sources (open circles). The red open squares indicate spectroscopically confirmed quasars (left), M1 quasar candidates (centre) and M2 quasar candidates (right).

therefore their nature is unknown. For the same reason, the value of the completeness is also indicative, as a complete spectroscopic coverage would alter both N_f and N_e.

4.2 Quasar candidates with WFS photometry

From the objects morphologically identified as point sources (SExtractor CLASS_STAR $\geqslant 0.9$) with detections at 15 μm, some 110 objects are part of the ELAIS Final Band-Merged Catalogue (Rowan-Robinson et al. 2004). M1 yields 27 quasar candidates with 18 spectroscopically confirmed, while M2 finds 63 candidates with 25 spectroscopically confirmed (Table 1). The two candidate lists have 27 objects in common, 18 of which are spectroscopically confirmed quasars. Taking into account condition C1, seven out of the 63 candidates proposed by M2 can be safely discarded as stars. Applying C2 on the remaining 56 candidates, we discard another five as more likely to be galaxies. Fig. 7 shows the positions of confirmed quasars and candidates, similar to Fig. 6, but for the WFS photometry.

The results obtained using WFS photometry are summarized in Table 3. As already mentioned, the values of completeness are underestimated due to lack of complete spectroscopic coverage.

After thorough consideration, we reach the conclusion that WFS data can be used in order to obtain quasar candidates reliably despite the issues raised by variability, especially if one combines M1 and M2 with the constraints imposed by the objects' IR properties.

4.3 Quasar photometric redshifts

For estimating the photometric redshifts, we applied a standard template fitting procedure using synthetic quasar spectra consisting of a power-law continuum and emission lines of fixed equivalent width values (Hatziminaoglou et al. 2000), on the sample of 73 spectroscopically confirmed quasars with both SDSS and WFS photometry available. The results are rather reliable when using SDSS photometry (53 out of 73 for $\Delta z \leqslant 0.2$, i.e. 73 per cent), but get worse when using the WFS photometry (29 out of 73 for $\Delta z \leqslant 0.2$, i.e. 30 per cent). Note, however, that all seven objects with spectroscopic redshifts lower than 0.3 have been assigned the wrong photometric redshifts. These objects, however, are extended (OBJC_TYPE = 3) and, therefore, their magnitudes [point spread function (psf) magnitudes for SDSS, and core magnitudes for WFS] must be contaminated by the light of the host galaxy. If we consider only the objects with spectroscopic redshifts higher than 0.3, the numbers of good identifications become 80 and 44 per cent, for SDSS and WFS, respectively. Furthermore, all 30 objects that were assigned correct photometric redshifts using the WFS photometry have also correct photometric redshifts when SDSS photometry is used. Fig. 8 illustrates the results obtained for SDSS (left-hand panel) and WFS (right-hand panel) photometry.

The fact that the bands for WFS photometry were taken in different periods of time (especially the *U* band, which was taken more than 2 yr apart in some cases) lead us to the conclusion that variability might be the basis of the discrepancy problem we encountered, as described in Section 3.

A case-by-case study of all objects that have correct photometric redshift estimates with SDSS photometry and bad estimates ($\Delta z > 0.25$) with WFS photometry showed that they all lie in the redshift range [0.3, 2.0] and their differences in magnitudes span a much larger range than the one expected due to the differences in the filters. One finally concludes that the wrong photometric redshift assignments are most probably due to variability, as argued earlier.

Table 3. Comparison of the completeness and confirmation rate yielded by M1 and M2 on a sample of 110 WFS point sources with 15-μm emission. The second column shows the number of quasar candidates (N_c) and the number of spectroscopically confirmed quasars among them (N_f).

Method	N_c (N_f)	Completeness	Conf. rate
M1	27 (18)	72 per cent	67 per cent
M2	63 (25)	100 per cent	42 per cent
M2 + C1	56 (25)	100 per cent	45 per cent
M2 + C1 + C2	51 (25)	100 per cent	49 per cent

5 COMPARISON BETWEEN IR DETECTED AND NON-DETECTED QUASARS

Thirty-six spectroscopically confirmed quasars lie in the parts of the ELAIS N1 and N2 fields covered by the SDSS spectroscopic data release, with 16 of them detected at 15 μm, as already mentioned. Considering the homogeneous way the SDSS quasar candidates are selected (Richards et al. 2002), we can ask if the two subsamples (16 IR and 20 non-IR emitters) have the same properties or if the IR detected quasars are, in some way, different. The colour–redshift (Fig. 9) and colour–colour (Fig. 10) diagrams of the two subsamples do not show any differences.

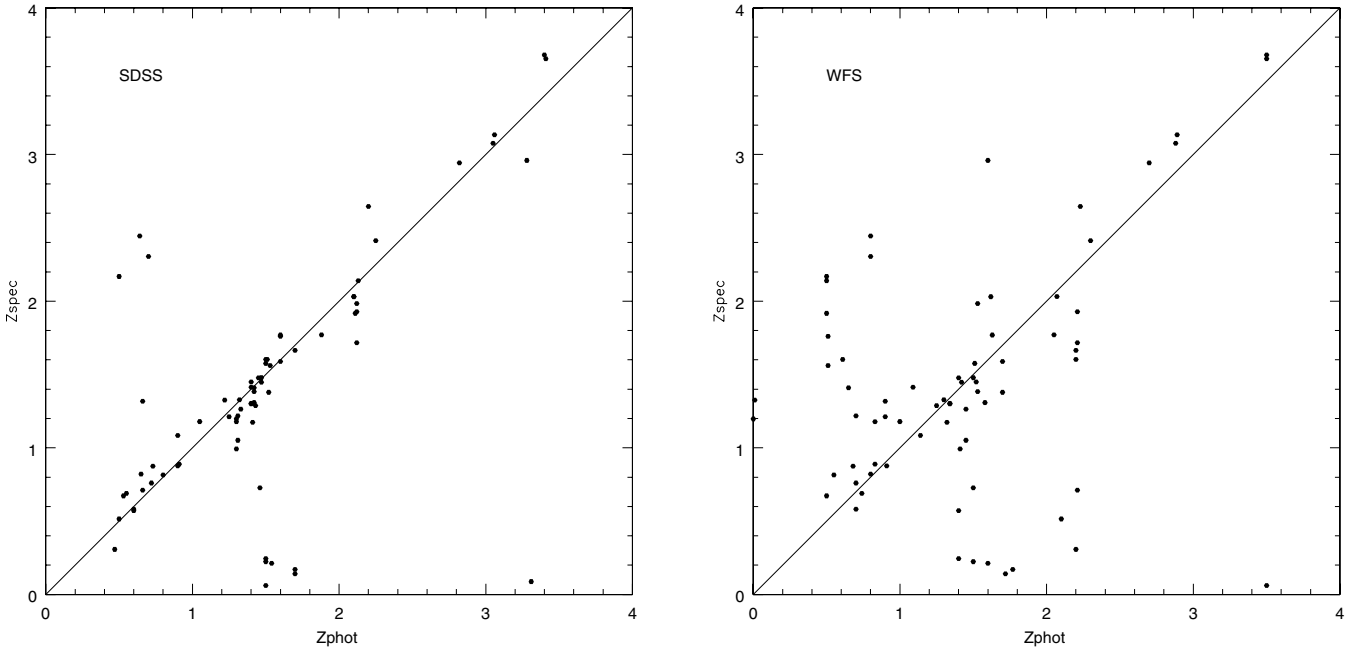

Figure 8. Photometric versus spectroscopic redshifts for the 73 SDSS quasars within the ELAIS N1 and N2 areas, using SDSS (left) and WFS (right) photometry. The larger scatter in the right-hand plot is most likely due to quasar variability – see text for details.

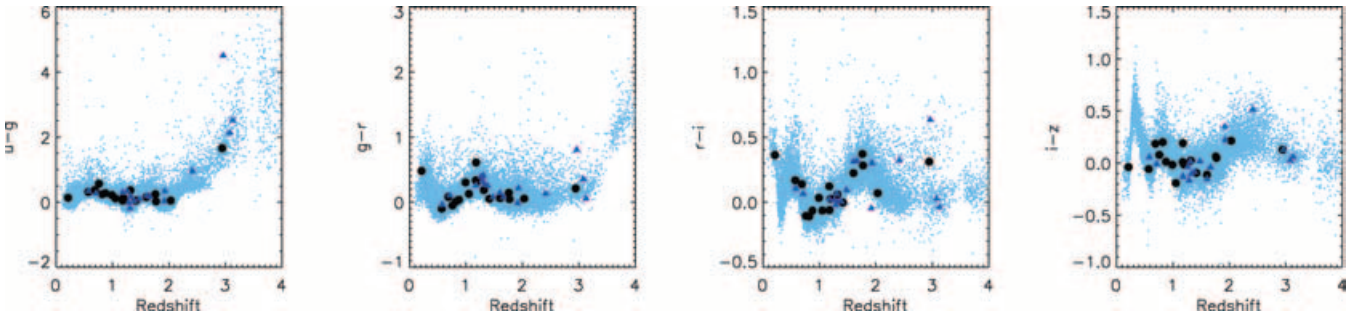

Figure 9. Colour–redshift diagrams for SDSS DR1 quasars (small dots), non-ELAIS quasars (triangles) and ELAIS quasars (filled circles).

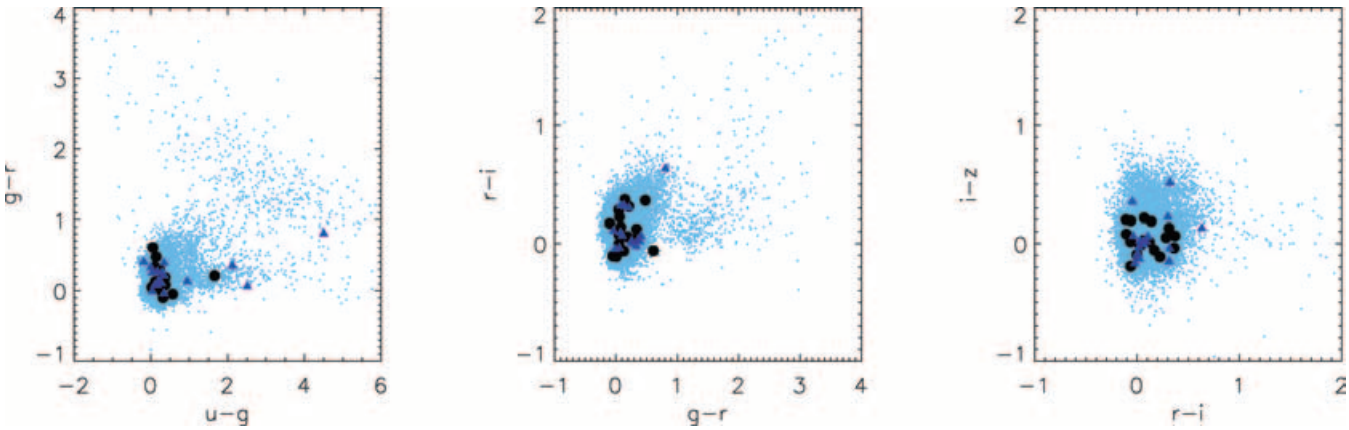

Figure 10. Colour–colour diagrams for SDSS DR1 quasars (small dots), non-ELAIS quasars (triangles) and ELAIS quasars (filled circles).

A two-sided Kolmogorov–Smirnov test on the BH mass distributions of the two subsamples (seen in the right-hand panel of Fig. 11) resulted in a larger than 90 per cent probability for them to come from the same population. The same test gave a 35 per cent probability for the redshift distributions to be representative of the same population. The largest deviation is noticed in the *r*-band magnitude distributions (left-hand panel of Fig. 11). The objects not detected by *ISO* at 15 μm are on average half a magnitude fainter

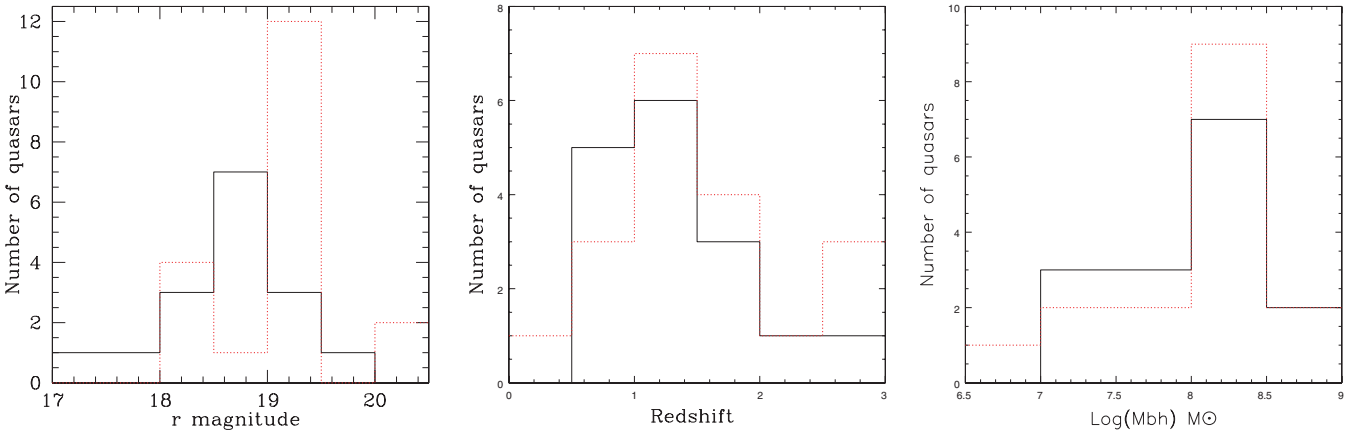

Figure 11. Histograms of *r*-band magnitude (left-hand panel), redshift (middle panel) and black hole mass (right-hand panel) for the ELAIS (black solid line) and non-ELAIS (red dotted line) quasars.

in the *r* band. Fig. 2 indicated a possible correlation between the 15-μm fluxes of the SDSS quasars and their optical (*r*-band) fluxes, suggesting that the lack of 15-μm counterparts could be due to their fainter magnitudes. Deeper IR observation would, presumably, provide counterparts for the remaining objects, since, for a given covering fraction and varying bolometric luminosity, brighter optical AGN should have a higher mid-IR emission.

5.1 Quasar black hole masses

The principal assumption underlying the BH virial mass estimate is that the dynamics of the broad-line region (BLR) are dominated by the gravity of the central supermassive black hole. Under this assumption, an estimate of the central BH mass, $M_{\rm BH}$, can be $M_{\rm BH} \simeq R_{\rm BLR}V^2/G$, where $R_{\rm BLR}$ is the radius of the BLR and V is the velocity of the line-emitting gas, traditionally estimated from the full width at half-maximum (FWHM) of the Hβ emission line (see Kaspi et al. 2000). For quasars with redshifts higher than typically $z \sim 0.8$, when Hβ is no longer available, McLure & Jarvis (2002) suggested the use of Mg II as an estimator of the BH mass. More precisely, the BH mass is computed as follows (McLure & Dunlop 2004):

$$\frac{M_{\rm BH}}{\rm M_\odot} = 4.7 \left(\frac{\lambda L_{5100}}{10^{37}\,\rm W}\right)^{0.61} \left[\frac{\rm FWHM(H_\beta)}{\rm km\,s^{-1}}\right]^2 \quad (1)$$

and

$$\frac{M_{\rm BH}}{\rm M_\odot} = 3.2 \left(\frac{\lambda L_{3000}}{10^{37}\,\rm W}\right)^{0.62} \left[\frac{\rm FWHM(Mg\,II)}{\rm km\,s^{-1}}\right]^2. \quad (2)$$

For the sample of 36 SDSS quasars in N1 and N2, therefore, low-redshift (up to ∼0.8) mass estimates are based on the correlation between the Hβ and the monochromatic luminosity at 5100 Å (equation 1), while for higher-redshift ones the correlation between Mg II and luminosity at 3000 Å (equation 2) is used. For objects with redshifts higher than 2, all estimators fall outside the covered wavelength range and BH masses can no longer be computed. Only objects with SDSS spectra were used for the BH mass computation, as line and continuum of all SDSS spectra are measured in a consistent way by the SDSS pipeline.

Fig. 12 shows the distribution of BH mass as a function of redshift. Red symbols mark the objects for which Hβ was used (with redshifts typically lower than ∼0.8), while black symbols illustrate those for which Mg II was considered. Filled 'circles' denote the objects with 15-μm emission, while 'triangles' correspond to SDSS objects within the ELAIS fields but without IR detections. BH masses show no differences between the two subsamples and follow the distributions found for the entire SDSS DR1 quasar catalogue by McLure & Dunlop (2004). The right-hand panel of Fig. 11 shows the BH mass histogram for the two subsamples, clearly indicating that both of them belong to the same parent population.

For the objects for which the 15-μm fluxes were available, their IR luminosity was computed assuming an $(\Omega, \Lambda) = (0.3, 0.7)$ cosmology. Fig. 13 shows the 15-μm IR luminosity of these objects as a function of redshift (left-hand panel) and as a function of the BH mass (right-hand panel). Clearly, high-mass BHs tend to produce higher IR luminosities. Furthermore, the IR luminosity versus redshift distribution compares nicely to the findings of Pozzi et al.

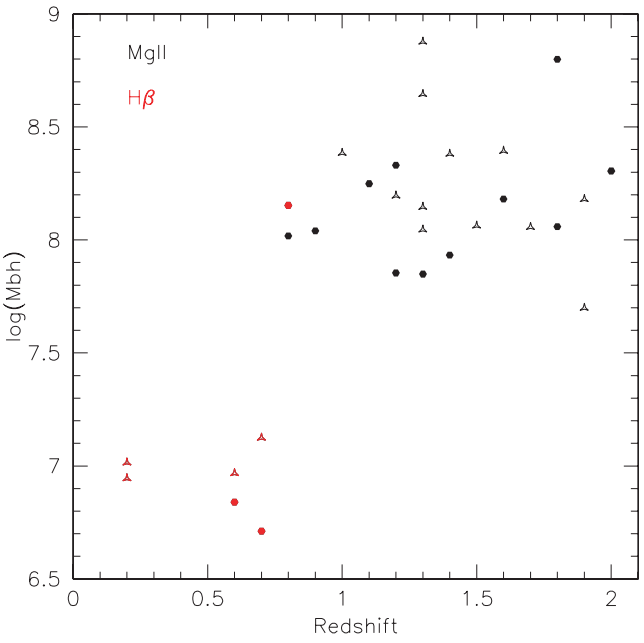

Figure 12. Black hole mass as a function of redshift for the ELAIS quasars with SDSS spectra (filled 'circles') and for the SDSS quasars without ELAIS counterparts ('triangles').

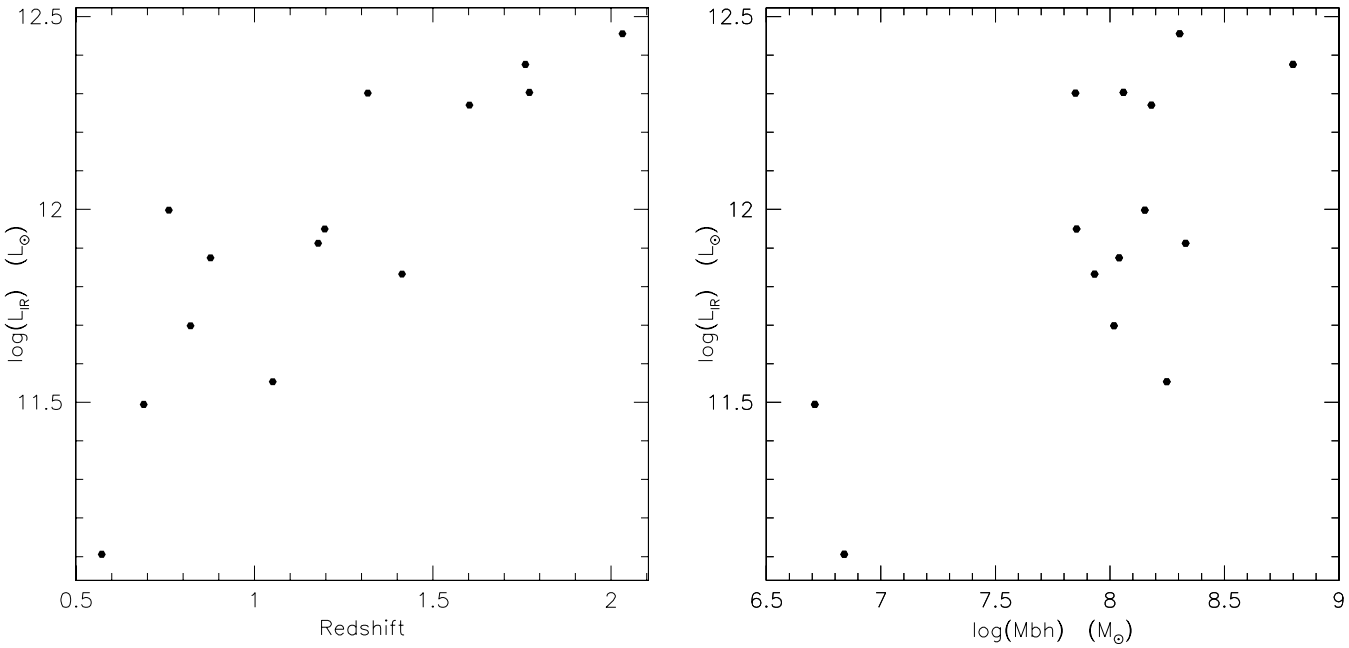

Figure 13. Plots of 15-μm IR luminosity of these objects as a function of redshift (left-hand panel) and as a function of the BH mass (right-hand panel).

(2003), indicating that Type I AGN in the redshift range [1, 2] have IR luminosities higher than 10^{12} $L_{\odot}$ (see fig. 6 of Pozzi et al. 2003), thus proving that *ISO* only skimmed the brighter end of the luminosity function.

6 DISCUSSION

This paper discusses some properties of the ELAIS 15-μm quasars and tries to establish a robust method of quasar selection for future use within the SWIRE framework. The importance of good-quality ground-based data is stressed, both for the selection of candidates and for the estimation of photometric redshifts. Colour–colour plots and template fitting are used for these purposes. Colour–colour plots give a higher confirmation rate, as expected, since they were trained on the same photometric system, while template fitting has the advantage of being independent of the filters used. The SDSS data have proved to be a reliable data set, while the WFS data are somewhat less efficient as a result of the large time-scales over which the imaging has been carried out and the variability issues that this introduced. In order to correct for these effects, the IR and optical to IR properties of the objects have been taken into account by imposing additional constraints on the quasar candidate selection techniques. The two subsamples of spectroscopically confirmed quasars detected and non-detected at 15 μm have been examined and they have shown no intrinsic physical differences. Their non-detection is most probably due to their fainter magnitudes, probably correlated to their higher redshifts.

This work can be seen as a validation of the tools and methods that will be used in the framework of SWIRE or other similar IR surveys supported by ground-based optical data. SWIRE will survey six high-latitude fields (including ELAIS N1 and N2), totalling 50 deg^2 in all seven *Spitzer* bands. One of the key scientific goals of SWIRE is to determine the evolution of quasars in the redshift range $0.5 \leqslant z \leqslant 3$ (Lonsdale et al. 2004). As we suggested in Section 5, with deeper IR observations one could detect all the quasars in the discussed fields down to the optical magnitude limit. In particular, the SWIRE 5σ photometric sensitivity is 0.0037 mJy in the IRAC 8-μm band and 0.15 mJy in the MIPS 24-μm band, much deeper than the characteristic depth of ∼1 mJy of ELAIS 15 μm (Vaccari et al. 2004). Last but not least, the multitude of the SWIRE bands will allow for a much better galaxy–AGN separation in the mid-IR colour space, possibly making the optical morphological preselection of quasar candidates obsolete.

Models (e.g. Granato & Danese 1994; Nenkova, Ivezic & Elitzur 2002) and observations (e.g. Elvis et al. 1994) suggest that quasar IR spectra are more or less flat (in νL_{ν}) from ∼1 μm down to at least 25 μm, even in the absence of starburst activity. Therefore, the deeper and better-quality SWIRE 8- and 24-μm observations will allow the detection of high numbers of quasars and the easy adaptation of the tools presented here. The stellar contamination will probably be higher at 8 than at 15 μm, but this problem will most likely be solved due to the multitude of IR bands, which will allow an easier separation of the galactic and extragalactic populations.

As a last remark, we would like to stress that a robust candidate selection technique and subsequent photometric redshift estimates such as the ones presented here will be increasingly required by all future large-area surveys, as spectroscopic coverage will never reach the same completeness, neither in area nor in depth.

ACKNOWLEDGMENTS

This paper is based on observations with *ISO*, an ESA project, with instruments funded by ESA Member States and with participation of ISAS and NASA. This work made use of data products provided by the CASU INT Wide Field Survey and the Sloan Digital Sky Survey. The INT and WHT telescopes are operated on the island of La Palma by the Isaac Newton Group in the Spanish Observatorio del Roque de los Muchachos of the Instituto de Astrofisica de Canarias. The SDSS website is http://www.sdss.org/. This work was supported in part by the Spanish Ministerio de Ciencia y Tecnologia (Grants Nos PB1998-0409-C02-01 and ESP2002-03716) and by the EC network 'POE' (Grant No HPRN-CT-2000-00138).

REFERENCES

Abazajian K. et al., 2003, AJ, 126, 2081
Bolzonella M., Miralles J.-M., Pelló R., 2000, A&A, 363, 476
Cesarsky C. et al., 1996, A&A, 315, L32
Elvis M. et al., 1994, ApJ, 95, 1
González-Solares E. A. et al., 2004, MNRAS, submitted
Granato G. L., Danese L., 1994, MNRAS, 268, 235
Hatziminaoglou E., Mathez G., Pelló R., 2000, A&A, 359, 9
Hatziminaoglou E. et al., 2002, A&A, 384, 81
Huber M. E., Clowes R. G., Soechting I. K., Howell S. B., 2002, Am. Astron. Soc. Meeting 210, 146.02
Kaspi S., Smith P. S., Netzer H., Maoz D., Jannuzi B. T., Giveon U., 2000, ApJ, 533, 631
Kessler M. F. et al., 1996, A&A, 315, L27
Lemke D. et al., 1996, A&A, 315, L64
Lonsdale C. et al., 2003, PASP, 115, 897
Lonsdale C. et al., 2004, ApJS, in press
McLure R., Dunlop J. S., 2004, MNRAS, 352, 1390
McLure R., Jarvis M. J., 2002, MNRAS, 337, 109
McMahon R. G., Walton N. A., Irwin M. J., Lewis J. R., Binclark P. S., Jones D. H., 2001, New Astron. Rev., 45, 97
Nenkova M., Ivezic Z., Elitzur M., 2002, ApJ, 570, 9
Oliver S. et al., 2000, MNRAS, 316, 749
Pozzi F. et al., 2003, MNRAS, 343, 1348
Richards G. T. et al., 2001, AJ, 122, 1151
Richards G. T. et al., 2002, AJ, 123, 2945
Rowan-Robinson M., 2001, New Astron. Rev., 45, 631
Rowan-Robinson M. et al., 2004, MNRAS, 351, 1290
Schneider D. P. et al., 2003, AJ, 126, 2579
Stoughton C. et al., 2002, AJ, 123, 485
Vaccari M. et al., 2004, MNRAS, submitted (astro-ph/0404315)
Vanden Berk D. E. et al., 2001, ApJ, 122, 549
Vanden Berk D. E. et al., 2004, ApJ, 601, 692

This paper has been typeset from a TEX/LATEX file prepared by the author.